American Mineralogist, Volume 59, pages 319–334, 1974

The Electronic Structure of Rutile, Wustite, and Hematite from Molecular Orbital Calculations

J. A. TOSSELL,[1] D. J. VAUGHAN,[2]

Department of Earth and Planetary Sciences, Massachusetts Institute of Technology

K. H. JOHNSON

Department of Metallurgy and Materials Science, Massachusetts Institute of Technology

Abstract

Molecular orbital (MO) calculations are presented for metal-oxygen polyhedral clusters containing Ti^{4+}, Fe^{2+}, and Fe^{3+} in octahedral coordination with oxygen. These polyhedra are used as models for the minerals rutile, wustite, and hematite. The calculations are used to elucidate the nature of the electronic structure of these minerals and to assign and interpret their X-ray and UV photoelectron, X-ray emission and absorption, and optical absorption and reflectance spectra. In all cases agreement with experiment is good. Comparisons are made between the Fe^{2+} and Fe^{3+} octahedral clusters using the calculations and X-ray emission and optical spectral data. Variations in the energies and intensities of peaks in the Fe$K\beta$, FeL and O$K\alpha$ X-ray emission spectra are adequately explained by the calculations. Spectral methods for determining the energies of the different MO's are suggested, and necessary conditions for the spectral assessment of mineral stability are discussed.

Introduction: Chemical Bonding Models for Transition Metals in Oxides and Silicates

The nature of chemical bonds involving transition metals in oxide and silicate minerals is of great importance to mineralogists because of its effect upon the chemical and physical properties of minerals. These in turn influence the nature of the physical processes studied by geophysicists. Although such concepts as ionic radius are very useful in explaining the coordination symmetries of transition metal ions in oxide and silicate minerals (Pauling, 1929, 1960), the systematics of element fractionation and site enrichment and the optical absorption spectra of transition metal bearing minerals can be explained only through the use of quantum mechanics (Burns, 1970; Burns and Fyfe, 1967). The quantum mechanical methods usually employed are those of atomic quantum mechanics, commonly in the form of crystal field theory (Bethe, 1929; Orgel, 1952). Crystal field theory has very successfully explained the optical absorption spectra of minerals, and the concept of the crystal field stabilization energy has been instrumental in explaining element partitionings and site enrichments.

It is well known, however, that crystal field theory is not a completely adequate theory for transition metal compounds. It describes only the predominantly metal d or "crystal field" orbitals but ignores the substantial covalency present in these compounds (Cotton and Wilkinson, 1972). The evidence for covalency ranges from the presence of transferred hyperfine splittings in the ESR spectra of transition metal compounds to the failure of the Born-Mayer lattice-energy equation for the accurate calculation of heats of formation of transition metal oxides (Gaffney and Ahrens, 1970). Another important evidence of covalency is the reduction of the Racah B and C interelectronic repulsion parameters in the spectra of oxides and silicates containing transition metals when compared to their free ion values (Manning, 1970). This effect arises from covalency but may be accommodated within the ligand field theory, which is essentially a parameterized modification of crystal field theory (Orgel, 1960).

Although molecular quantum mechanics is therefore *formally* necessary for the description of the

[1] Present address: Division of Geochemistry, Department of Chemistry, University of Maryland, College Park, Maryland 20742.

[2] Present address: Department of Geological Sciences, University of Aston, Gosta Green, Birmingham B47ET, England.

electronic structure of transition metal compounds, it has been little employed in mineralogy for two reasons. First, the electrons most easily studied experimentally have been the *d* electrons of the transition metal, and the optical absorption spectra generated by transitions between them could be described fairly well by crystal field or ligand field theory. Second, crystal field theory provided a well-defined quantitative method for obtaining information on energetics from optical spectra at a time when quantitative molecular quantum mechanics afforded little agreement either between different molecular quantum mechanical calculations or between calculation and experiment. It was possible to use qualitative molecular orbital theory but in practice the qualitative theory was ambiguous and unconvincing.

Both reasons for not using molecular quantum mechanics in mineralogy have now largely lost their validity. New types of spectroscopy which yield information on electrons other than those of the metal *d* shell have been developed and applied to minerals. Important examples include X-ray emission studies (Urch, 1971), and the X-ray absorption and photoelectron (Nordling, 1972) spectroscopies discussed below. Qualitative MO theory has been used to interpret X-ray emission spectra for some time (Dodd and Glenn, 1969; Smith and O'Nions, 1972a, 1972b), but such interpretations are necessarily uncertain. Fortunately, at the same time as new spectral methods were being applied in mineralogy, new quantum mechanical methods and computer programs were being developed to yield electronic wave-functions in much closer agreement with experiment than formerly. Substantial advances have been made in the application of the traditional Hartree-Fock-Roothaan Self Consistent Field Linear Combination of Atomic Orbitals-Molecular Orbital (HFR SCF LCAO-MO) theory (Roothaan, 1951) to transition metal complexes (Moskowitz *et al,* 1970; Clack *et al,* 1972). Approximate semi-empirical LCAO-MO theory has been successfully applied to the study of the geometries and energetics of several classes of silicate minerals (Louisnathan and Gibbs, 1972). Similar calculations have been used with reasonable success to interpret the X-ray emission spectra of oxide minerals containing Mg, Al, and Si (Tossell, 1973a, b) and of Be and B oxyanions (Vaughan and Tossell, 1973). The metal $K\beta$ and $OK\alpha$ X-ray emission spectra of these minerals contain valuable information on the stabilities of the bonding orbitals as a function of chemical and geometrical parameters. The success of these approximate calculations is in part a result of the relative simplicity of the systems studied. For transition metal systems, however, more sophisticated methods are required. In this work, a new first-principles molecular orbital approach, namely the SCF $X\alpha$ Scattered Wave Cluster Method (Slater and Johnson, 1972; Johnson and Smith, 1972; Johnson, 1973), is used. This method yields molecular orbitals for transition metal compounds which are in better quantitative agreement with experiment than those obtained from *ab initio* LCAO calculations (Johnson, 1973).

Molecular quantum mechanical calculations using the SCF $X\alpha$ method on polyhedral clusters containing Ti^{4+}, Fe^{2+}, and Fe^{3+} in octahedral coordination with oxygen are reported in this paper. In the next section, the SCF $X\alpha$ method will be described and then the various spectral methods briefly discussed. The molecular orbital results and spectral interpretations for TiO_2 (rutile), FeO (wustite), and Fe_2O_3 (hematite) will then be presented. In the final section, a general discussion will be given of the electronic structure of oxides of transition metals and of spectral methods for studying the nature of the electronic structure and for assessing mineral stability.

Calculational Method

The SCF $X\alpha$ method is a computationally efficient, first-principles molecular orbital method based on the division of matter into component polyatomic clusters (Johnson, 1973). In this respect it is similar to the model of Pauling (1929). For example the SCF $X\alpha$ model for rutile (TiO_2) is the TiO_6^{8-} cluster, a Ti^{4+} ion surrounded by six O^{2-} ions. This model should also be appropriate for Ti^{4+} in any octahedral site, for example, those in ilmenite and titanaugite.

The seven steps in the method are:

(1) The space within and around the cluster is geometrically partitioned into three contiguous regions, namely, (I) the atomic regions, spherical regions centered on each of the atomic nuclei and touching along the metal-ligand axis, (II) the interatomic region, the region outside the atomic regions but within an "outer sphere" enclosing all the atomic spheres, and (III) the extramolecular region, the region beyond the "outer sphere." Also, the electrostatic potential of the re-

maining atoms in the crystalline lattice is approximated by a spherical shell of positive charge (the "Watson sphere"), that is equal in magnitude to the charge of the cluster and that passes through the nuclei of the ligands in the cluster. After the calculation is completed, a correction is made to the absolute values of the orbital energies equal to the difference between the "Watson sphere" stabilization and the accurate Madelung potential (Vaughan, Tossell, and Johnson, 1974).

(2) The potential energy at each point is then evaluated, using electrostatics to calculate the Coulomb part of the potential and the $X\alpha$ statistical approximation of Slater (1972) to evaluate the exchange-correlation contribution. The $X\alpha$ approximation employs a proportionality between the exchange-correlation potential at a point and the cube root of the density of like-spin electrons at that point. The proportionality constant, α, in this approximation is determined from first principles for the component free atoms, these α values then being transferred to the corresponding atomic regions of the cluster. Appropriately weighted values of α are used in the interatomic and extramolecular regions (Johnson, 1973).

(3) The potential is simplified to a *muffin-tin* form by spherical averaging in the atomic and extramolecular regions and volume averaging in the interatomic region.

(4) The one-electron Schrödinger equation is solved numerically in each region and the solutions are expanded in a rapidly convergent composite partial-wave representation.

(5) The wavefunctions and their first derivatives are joined continuously throughout the various regions of the cluster using multiple-scattered-wave theory (Johnson, 1973).

(6) The spatial distribution of the electron density is calculated and is used to generate a new potential for the next step in the iterative process. The entire numerical procedure is repeated in successive iterations until self-consistency is attained.

(7) The final self-consistent solution for the ground state of the cluster is expressed in terms of one electron molecular orbitals. These are characterized by their orbital energies (or eigenvalues), by their occupation numbers, and by their electron density distributions.

The SCF $X\alpha$ method differs from the more familiar Hartree-Fock-Roothaan LCAO-MO method in two very important ways. First, in the SCF $X\alpha$ approach the Schrödinger equation is solved numerically rather than by expansion in a finite analytical atomic orbital basis set. LCAO methods require the choice of a finite basis set of atomic orbitals and the size of the basis set seriously affects the accuracy of the results. Second, in Hartree-Fock theory, as a result of the HF treatment of the exchange potential, the empty orbitals are treated as "virtual" orbitals which encounter their own self-repulsion and are therefore somewhat too diffuse (Huzinaga and Arnau, 1971). In the SCF $X\alpha$ method, the filled and empty orbitals are treated equivalently by the $X\alpha$ approximation so that the empty orbitals are good representations of excited state orbitals.

The method has previously been applied to two important minerals; SiO_2, α-quartz (Tossell, Vaughan, and Johnson, 1973a) and Fe_2O_3, α-hematite (Tossell, *et al*, 1973b). A companion paper discussing the electronic structure of Fe^{2+} in tetrahedral coordination with oxygen and sulfur is in press (Vaughan, Tossell, and Johnson, 1974). For the SiO_4^{4-} molecular cluster, the SCF $X\alpha$ model for α-quartz, good agreement was found with the experimental X-ray photoelectron, Si$K\beta$ and O$K\alpha$ X-ray emission and UV spectra of quartz. The valence region MO's of SiO_4^{4-} were found to be divisible into three filled sets: (1) O 2*s* nonbonding orbitals ($4a_1$ and $3t_2$); (2) Si 3*s*, 3*p* and O 2*p* bonding orbitals ($5a_1$ and $4t_2$, separated by 3–4 ev); and (3) O 2*p* nonbonding orbitals ($1e$, $5t_2$,$1t_1$), closely spaced in energy, and an empty set (4) diffuse Si-O antibonding orbitals ($6a_1$, $6t_2$). No significant Si 3*d* participation was found in either the O 2*p* nonbonding orbital set or in the bonding orbital set. The small calculated separation of the nonbonding orbitals was in good agreement with the experimental X-ray photoelectron data (DiStefano and Eastman, 1971). LCAO calculations, which found much greater Si 3*d* participation, obtained erroneously high values for the energy separation of these orbitals (Collins, Cruickshank, and Breeze, 1972). It appears that the large Si 3*d* participation found in this LCAO calculation is therefore an artifact of the inadequacy of the basis set used. This is supported by the SCF LCAO results of Gilbert *et al* (1973) who find a maximum of 5 percent Si 3*d* participation in the MO's of Si_2O using a larger basis set. Using the X-ray photoelectron,

X-ray emission, and UV spectra of SiO_2 together with the SCF $X\alpha$ calculation, it was possible to determine the positions of all the orbitals in the system, usually to within one electron volt. We have recently learned that high resolution $OK\alpha$ spectra of SiO_2 (Klein and Chun, 1972) show a main peak (arising from the $1t_1$ orbital) and three features at lower energy which can be identified with the $1e + 5t_2$, $4t_2$ and $5a_1$ orbitals (the existence and energy of the weak $5a_1$ peak confirming the prediction of Urch, 1970). This interpretation is consistent with the X-ray photoelectron data of DiStefano and Eastman (1971) and with the SCF-$X\alpha$ calculation.

Spectroscopic Study of Electronic Structure of Transition Metal Oxides and Silicates

Optical absorption spectroscopy, and related techniques such as diffuse reflectance spectroscopy, give information on the relative energies of the highest occupied and lowest empty orbitals in transition metal oxides and silicates. Experimental spectral energies may be used to define parameters, such as 10 Dq, which can be used within the framework of crystal field theory to assess the stability of metal-oxygen polyhedra (Burns, 1970). The major deficiencies of optical absorption spectroscopy are the small range of energies spanned by the technique and the complexity of the spectra. The range of energies studied can be expanded by the use of UV reflectance spectroscopy. The UV reflectance technique is of particular value for studying ligand → metal charge-transfer spectra.

In X-ray emission spectroscopy, an electron is ejected from a core orbital by an X-ray or an energetic electron. A higher energy outer electron then drops into the core "hole" and a photon is generated with energy approximately equal to the difference in eigenvalue (energy) of the outer and core orbitals. X-ray emission spectroscopy may be used to study both the inner shells and the valence regions of transition-metal oxides. Systematic studies have been made of transition-metal oxide $K\beta$ (Köster and Mendel, 1970) and L (Fischer, 1971, 1972) X-ray emission spectra. X-ray emission spectra are often easier to interpret than optical spectra because there are fewer spectral features spread over a wider energy range and because symmetry selection rules are more rigorously followed. The major deficiencies in the X-ray emission technique are in the poor energy resolution (although important advances have recently been made by Werme *et al,* 1973) and in the need to superimpose several different series of X-ray emission and absorption spectra to determine the positions of all the MO's of the material. This requires that a common energy scale be constructed (Fischer, 1971).

In photoelectron spectroscopy, a "photoelectron" is ejected by an incident photon. Its kinetic energy is measured accurately, and the photon energy less the photoelectron kinetic energy gives the binding energy (~ the negative of the eigenvalue) of the orbital from which the electron was ejected. X-ray and UV photoelectron spectra show intensity from all the orbitals in the valence region of a material. However, on all but the newest machines, the spectral resolution is often insufficient to show much structure in the valence region (*e.g.,* Prins and Novakov, 1972) and complications can arise from satellite peaks (Hüfner and Wertheim, 1973).

X-ray photoelectron spectroscopy can also be used to study the shifts of inner-shell orbital energies yielding information on molecular charge distributions. However, as opposed to X-ray emission inner-orbital spectra, which show shifts only as a function of oxidation state and nearest neighbor coordination, the inner-shell photoelectron peaks are significantly influenced by charges on distant atoms (Shirley, 1970). The influence of distant charges and the problems associated with sample charging and reference level effects make the interpretation of inner-shell energy shifts for minerals very difficult (Adams, Thomas, and Bancroft, 1972).

The spectral techniques discussed above are largely complementary, and an adequate wavefunction should be capable of explaining all the observed spectra. The purpose of using SCF $X\alpha$ wavefunctions to interpret the spectra of minerals is twofold. First, an adequate explanation of the spectra establishes the validity of the calculation. Second, the interpretations of the spectra are clarified, making it possible to identify those spectral features which yield the most direct information about the nature of the bonding and other quantities of interest.

The Electronic Structure and Spectra of Rutile, TiO_2

Titanium, the second most abundant transition metal in the earth's crust, is commonly found as the TiO_2 polymorph, rutile. Its oxidation state is

usually +4 and its coordination is commonly six-fold, although +3 oxidation and four-fold coordination do occur. Rutile is tetragonal, but the distortion of the coordination polyhedra is fairly small (2 Ti-O distances are 1.988 Å; 4 are 1.944 Å), (Grant, 1959) and should have little effect upon the spectra.

MO Diagram for TiO_6^{8-}

The calculated MO diagram for the TiO_6^{8-} molecular cluster is shown in Figure 1. Although all electrons of the cluster (78 for TiO_6^{8-}) are included in the SCF $X\alpha$ calculation, only the O 2*s* type orbitals and the valence orbitals are shown in the MO diagram, since the orbitals of lower energy are essentially atomic in nature. The orbital energies are given in *ev* and the energy levels of the free atoms (from atomic SCF $X\alpha$ calculations) are included for comparison. The orbitals are labeled according to the irreducible representations of the octahedral (O_h) group under which they transform. These O_h representations are such that the central atom *s* orbitals belong to the a_{1g} representation, the *p* orbitals belong to t_{1u}, and the *d* orbitals belong to e_g and t_{2g}. Appropriate symmetry combinations of the ligand orbitals belong to all the irreducible representations. The SCF $X\alpha$ program calculates the electron density in each region of the molecular cluster and such quantities as the amount of "Ti 3*d*" character in an e_g MO can be assessed from the percent electron density inside the Ti sphere.

The MO's in TiO_2 and other transition metal oxides fall into five sets, distinguishable by their energies and by the spatial distribution of their electron density. The orbitals with eigenvalues around −22 ev ($5a_{1g}$, $4t_{1u}$, $1e_g$) are essentially O 2*s* nonbonding orbitals with a slight metal-orbital admixture. The main bonding orbitals of the system—$5t_{1u}$, $6a_{1g}$, $1t_{2g}$, and $2e_g$—possess appreciable metal and oxygen character. A strong indication of the bonding nature of these orbitals is the large amount of electron density in the interatomic region (~30–40 percent). The $1t_{2u}$, $6t_{1u}$, and $1t_{1g}$ orbitals are all primarily O 2*p* nonbonding orbitals with relatively little metal character and little density in the interatomic region. The $1t_{1g}$ is the highest-energy filled orbital. The two lowest-energy empty orbitals are the $2t_{2g}$ and $3e_g$ "crystal field" orbitals, which have both Ti 3*d* and O 2*p* character. The empty orbitals of the conduction band—$7a_{1g}$ and $7t_{1u}$—are diffuse Ti-O antibonding orbitals. The

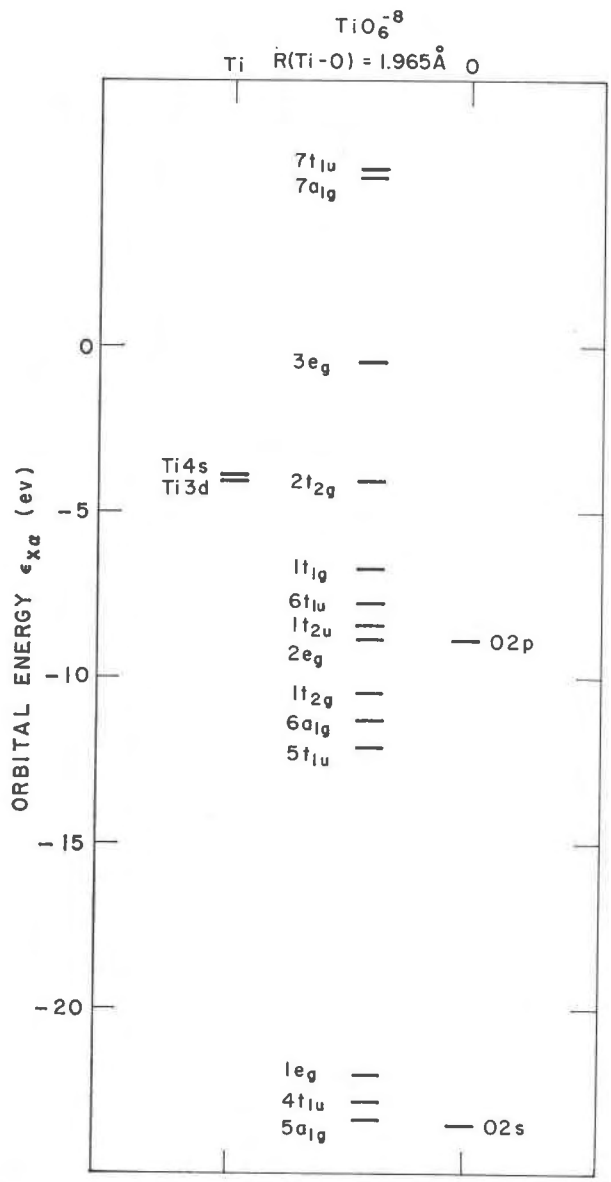

FIG. 1. TiO_6^{8-} *MO* diagram (R(Ti − O) = 1.965 Å); the highest occupied orbital is the $1t_{1g}$.

spatial distributions of the orbitals are listed in Table 1. For no orbital is there as much as 1 percent density in the extramolecular region (III), so this region has been omitted from the table.

The TiO_6^{8-} MO diagram differs from traditional textbook MO diagrams in the following respects. The order of the t_{2g} and e_g orbitals is the same in both the bonding and crystal field sets and the a_{1g} and t_{1u} orbital energies are quite similar in both the bonding and conduction band sets. There is also a well-defined set of O 2*p* nonbonding orbitals.

TABLE 1. Percentage Spacial Distribution of Electron Density in TiO_6^{8-} *MO*'s

	REGION I		REGION II
	Ti	O	(interatomic)
	Ti-O antibonding orbitals		
$7t_{1u}$	1	37	62
$7a_{1g}$	2	39	59
	Ti3d "crystal field" orbitals		
$3e_g$	69	31	0
$2t_{2g}$	69	18	13
	O2p nonbonding orbitals		
$1t_{1g}$	0	87	13
$6t_{1u}$	1	83	16
$1t_{2u}$	0	79	21
	Ti-O bonding orbitals		
$2e_g$	21	58	21
$1t_{2g}$	12	57	31
$6a_{1g}$	3	55	42
$5t_{1u}$	2	61	37
	O2s nonbonding orbitals		
$1e_g$	3	86	11
$4t_{1u}$	2	84	14
$5a_{1g}$	2	81	17

In general the orbitals are very much "grouped" rather than being continuously distributed as suggested by many qualitative MO diagrams. The only orbital not easily assignable to one of the orbital "sets" is the $2e_g$ (Ti-O "σ-bonding") which has an energy and charge distribution intermediate between those characteristic of the bonding and O $2p$ nonbonding sets.

TABLE 2. Experimental and Calculated UV and X-ray Photoelectron Spectra of Rutile
(energies in ev)

Experimental peak label	Experimental relative E*	Calculated relative E	MO assignment
	UV Photoelectron Spectrum		
	0	0	$1t_{1g}$
O2p	-2.2	-1.5	$6t_{1u}$, $1t_{2u}$, $2e_g$
O2s**	-4.8	-4.6	$1t_{2g}$, $6a_{1g}$, $5t_{1u}$
	X-ray Photoelectron Spectrum		
O2p	~5 ev wide	5.4 ev wide	$1t_{1g}$ - $5t_{1u}$
O2s	~-16 ev***	13.9 ev***	$1e_g$, $4t_{1u}$, $5a_{1g}$

* Experimental UV data from Derbenwick (1970); experimental X-ray data from Hüfner and Wertheim (1973).

** As shown by Fischer (1972), this labeling is definitely erroneous.

*** Relative E taken with respect to center of O2p peak (experimental) or to center of valence region (calculated).

Rutile: X-Ray and UV Photoelectron Spectra

Table 2 summarizes the observed X-ray (Hüfner and Wertheim, 1973) and UV (Derbenwick, 1970, reproduced in Fischer, 1972) photoelectron spectra of rutile. The resolution in the X-ray spectrum is lower because of the greater intrinsic width of the exciting X-ray line, but the width of the valence band is about 5 ev in both spectra. In the UV photoelectron spectrum, the bonding and O $2p$ nonbonding orbital sets in the valence band can be resolved.

There are experimental uncertainties in the absolute values of the photoelectron binding energies due to charging and reference level effects in TiO_2. In addition, our approximate treatment of the Madelung correction to the TiO_6^{8-} orbital energies precludes accurate calculation of absolute binding energies. Therefore in Table 2 we have simply set the energy of the $1t_{1g}$ orbital equal to that of the lowest-binding-energy photoelectron peak and adjusted the other orbital energies accordingly. The relative energies of the valence band orbitals appear to be reproduced quite well. The separation between the O $2s$ orbitals and the middle of the valence band we calculated to be about 14 ev, which compares favorably with the experimental X-ray photoelectron value of ~16 ev. Therefore the orbital energies in the O $2s$ and valence regions seem to be reproduced reasonably well by the SCF $X\alpha$ calculation.

Rutile: Optical Spectra

Table 3 shows the observed and calculated optical absorption and UV reflectivity spectra of rutile. Since Ti^{4+} has no d electrons, the optical absorption spectrum exhibits only an edge at 3.03 ev (Cronemeyer, 1952). An analogous peak is observed in the photoconductivity spectrum at about the same energy (Cronemeyer, 1952). For some time it has been assumed that the absorption edge in TiO_2 and related compounds arose from a ligand → metal charge-transfer transition (Kahn and Leyendecker, 1964). This is verified by our calculation which assigns the absorption edge to the $1t_{1g} \rightarrow 2t_{2g}$ transition, *i.e.*, O $2p$ nonbonding → Ti $3d$. In the SCF $X\alpha$ method, transition energies are calculated not from ground

state eigenvalue differences but by using the "transition state" concept of Slater (1972). In the "transition state", half an electron is considered to be excited from the initial into the final orbital and the calculation is then iterated to self-consistency for the "transition state" electronic configuration. The transition energy is expressed as the difference of the "transition state" eigenvalues of the initial and final states. Although this procedure is formally required for all types of spectral transitions, it seems to have a large effect on the relative spectral energies only for optical spectra. The calculated "transition state" energy for the $1t_{1g} \rightarrow 2t_{2g}$ excitation is 3.2 ev, in excellent agreement with experiment (the ground state excitation energy is 2.6 ev).

The UV reflectivity spectrum of TiO_2 is more informative than the optical absorption spectrum but somewhat more difficult to interpret. There are intense peaks at ~4.7 ev (A) and 8.8 ev (C), weaker sharp peaks at 14.0 ev (E) and 17.4 ev (F), a shoulder (D) at 10.7 ev, and some weaker peaks (B) noted by Cardona and Harbeke (1965). The possibility that peaks A and C result from transitions from the O $2p$ nonbonding orbitals to the $2t_{2g}$ and $3e_g$ orbitals, respectively, is unlikely because their separation is 4.1 ev whereas the "crystal field" splitting of the $2t_{2g}$ and $3e_g$ orbitals should be 2.7-2.9 ev for Ti^{4+} with a Ti-O distance of 1.959 Å (the crystal field splitting is equal to 2.5 ev for aqueous Ti^{3+}, with a slightly longer Ti-O distance (Figgis, 1966, p. 218)). A second possibility is that the $2t_{2g}$ orbital is the final state for both A and C and that the initial states are in the nonbonding and bonding orbital sets of the valence band, respectively. The calculated separation of the $6t_{1u}$ (O $2p$ nonbonding) and $5t_{1u}$ (bonding) orbitals, both of which can participate in symmetry-allowed transitions to the $2t_{2g}$ orbital, is 4.3 ev, in excellent agreement with the ~4.1 ev separation between peaks A and C. It was demonstrated in the previous section that our calculated valence orbital energies were in good agreement with the UV photoelectron spectrum; therefore the calculations and photoelectron spectra both support this assignment of peaks A and C in the reflectivity spectrum. Peaks E and F can also be adequately assigned to discrete transitions between MO's using the suggested qualitative assignments of Cardona and Harbeke (1965). The only peaks not readily assignable from our calculation are D (assigned by Cardona and Harbeke to O^{2-} $2p \rightarrow 3s$) and the weak B peaks, some of which

TABLE 3. Experimental and Calculated Optical Spectra of Rutile
(energies in ev)

Observed Feature	Experimental ΔE	Calculated ΔE	MO assignment
	Optical Absorption		
absorption edge	3.03*	3.2	$1t_{1g} \rightarrow 2t_{2g}$ (02p nb→Ti3d)
	UV Reflectivity		
Peak A	~4.7**	4.2, 4.8***	$(6t_{1u}, 1t_{2u}) \rightarrow 2t_{2g}$ (02pnb→Ti3d)
Peak C	~8.8	8.4	$5t_{1u} \rightarrow 2t_{2g}$ (Ti-Ob →Ti3d)
Peak D	10.7		O^{2-} 2p→3s
Peak E	14.0	13.3	$(6t_{1u}, 1t_{2u}) \rightarrow (7a_{1g}, 7t_{1u})$ (02pnb→Ti-O ab)
Peak F	17.4	18.5	$(1e_g, 4t_{1u}, 5a_{1g}) \rightarrow 2t_{2g}$ (02snb→Ti3d)

b, nb, and ab refer to bonding, nonbonding, and antibonding orbitals respectively.

* Cronemeyer (1952).

** Cardona and Harbeke (1965).

*** calculated as ground state transition energies +.5 ev by analogy with $1t_{1g} \rightarrow 2t_{2g}$

may be associated with transitions to the $3e_g$ orbital. Overall, the agreement of the calculated spectrum with experiment is quite good. It is clear that, if our interpretation is correct, the reflectivity spectrum gives direct information on the relative energies of all five orbital sets.

Rutile: X-Ray Emission and Absorption Spectra

In Table 4, the observed and calculated X-ray emission and absorption spectra of rutile are presented. Although the individual experimental spectra are the same as those used by Fischer (1972), there are some doubts about his energy alignment of the various spectral series and therefore each spectrum will be discussed individually.

The Ti$K\beta$ emission spectrum shows a number of peaks, which arise from transitions in which an electron in a t_{1u} (Ti p type) orbital drops into a hole in the Ti $1s$ shell. The main peak, $K\beta_1$, arises from the $3t_{1u}$ MO which is essentially a Ti $3p$ orbital. The satellite peak $K\beta'$ is assigned to a discrete energy-loss process in which a $K\beta_1$ photon excites an electron from the $1t_{2g}$ orbital into the $7t_{1u}$ orbital, *i.e.*, an exciton process. This interpretation is very similar to that suggested by Köster and Mendel (1970) on qualitative experimental grounds and yields good values for the relative $K\beta'$ energies in TiO_2, FeO, and Fe_2O_3. In particular the $7t_{1u}$ conduction band orbital is found to be at higher energy ($K\beta'$ lower with respect to $K\beta_1$) in TiO_2 than in the iron oxides and at higher energy in Fe_2O_3 than in FeO. The $K\beta''$

TABLE 4. Experimental and Calculated X-ray Emission and Absorption Spectra of Rutile
(energies in ev)

Experimental peak label	Experimental relative E*	Calculated relative E	MO assignment
	TiKβ Emission		
Kβ'	∿-16 (LB)	-15.8	$3t_{1u} \rightarrow$ Tils-($1t_{2g} \rightarrow 7t_{1u}$)
$K\beta_1$	0	0	$3t_{1u} \rightarrow$ Tils
Kβ"	15.2	17.1	$4t_{1u} \rightarrow$ Tils
$K\beta_5$	30.4, 29.7 (KM) (BS) 31.4	27.8	$5t_{1u} \rightarrow$ Tils
$K\beta_5$'		32.1	$6t_{1u} \rightarrow$ Tils
	TiL Emission		
F	0 (FI)	0	$1t_{1g} \rightarrow Ti2p_{3/2}$
A		-2.1	$2e_g \rightarrow Ti2p_{3/2}$
)	-4.2	-3.8	$1t_{2g} \rightarrow Ti2p_{3/2}$
G		-4.6	$6a_{1g} \rightarrow Ti2p_{3/2}$
C	-18.8	-15.3	$1e_g \rightarrow Ti2p_{3/2}$
D	-21.3	-16.7	$5a_{1g} \rightarrow Ti2p_{3/2}$
	OKα		
main peak	0	0	($1t_{1g}$, $6t_{1u}$, $1t_{2u}$, $2e_g$)→01s
low energy shoulder	-2.6 (OS) -2.7 (FI)	-3.4	($1t_{2g}$, $6a_{1g}$, $5t_{1u}$)→01s
	TiK, TiL, OK absorption**		
b	3.1	2.6	core hole→$2t_{2g}$
c	5.2	6.2	core hole→$3e_g$
d	11.5	12.5	core hole→$7a_{1g}$, $7t_{1u}$
e	18.9		

* Data from Landolt-Börnstein, 1955 (LB); from Koster and Mendel, 1970 (KM); from Blokhin and Shuvaev, 1962 (BS); from Fischer, 1972 (FI); and from O'Nions and Smith, 1972 (OS).

** E values calculated relative to $1t_{1g}$ (ground state energy differences).

peak clearly arises from the $4t_{1u}$ orbital, which resembles O 2*s*. The $K\beta_5$ peak is somewhat more difficult to assign definitively. The two $K\beta_5$ peaks observed by Blokhin and Shuvaev (1962) possibly correspond to the $5t_{1u}$ and $6t_{1u}$ orbitals. However, the experimental splitting of the $K\beta_5$ doublet is much smaller (∼1.7 ev) than the calculated $6t_{1u}$-$5t_{1u}$ separation (4.3 ev) or that inferred from the reflectivity spectrum (4.1 ev). It seems more probable that the $6t_{1u}$ 2*p* nonbonding orbital (with very little Ti 4*p* character) will generate only a weak feature, $K\beta_5$, similar to the weak high energy shoulder observed in the Si$K\beta$ spectrum of SiO_2 (Klein and Chun, 1972). The $K\beta$ spectrum of Blokhin and Shuvaev does show a weak shoulder at about the expected energy. The doubling of the $K\beta_5$ peak may arise from a splitting of the $5t_{1u}$ orbital. This may result from interaction between the metal-oxygen polyhedra (Tossell, 1973a).

The Ti$L\alpha$ spectrum (nominally arising from Ti 3*d*, 4*s* → Ti $2p_{3/2}$ transitions) shows two broad intense peaks with maxima separated by ∼4.2 ev. The higher-energy $L\alpha$ emission peak (designated F in Fischer, 1972) is assigned by us to a $1t_{1g} \rightarrow$ Ti2*p* transition. Fischer assigns this peak to the $1t_{2g}$ orbital, discounting the possibility of $1t_{1g}$ participation because neither the Ti 3*d* nor 4*s* orbitals belong to this representation. This approach employs the normal assumption that the selection rules governing X-ray emission are atomic in nature, *i.e.*, for *L* spectra the upper level must be an *s* or *d* state. However, we believe that the correct selection rules are actually *molecular* in nature, *i.e.*, determined by the O_h point group. Since the Ti 2*p* level and the dipole moment operator are both of t_{1u} character, the allowed upper states are therefore $a_{1g} + e_g + t_{2g} + t_{1g}$. The use of molecular selection rules admits the possibility that the highest filled orbital is in fact the $1t_{1g}$ and therefore removes the necessity for assigning the TiO_2 absorption edge to a symmetry-forbidden $1t_{2g} \rightarrow 2t_{2g}$ transition, as in Fischer (1972). In general we believe that in cases in which the upper atomic levels nominally involved in the X-ray transitions are filled (*e.g.*, the O 2*p* levels which generate intensity in the O$K\alpha$ emission spectrum) the atomic selection rules are adequate. However when the appropriate atomic levels are essentially empty (*e.g.*, Ti 3*d* and Ti 4*s* in TiO_2), absolute spectral intensities are reduced and transitions forbidden by the atomic selection rules—but weakly allowed by the molecular selection rules—can generate appreciable *relative* intensity and therefore yield spectral features.

The lower energy $L\alpha$ peak is resolved by Fischer into two components (A and G). Our calculations indicate that the $2e_g$, $1t_{2g}$, and $6a_{1g}$ orbitals have the proper energies to contribute to this peak. The peak maximum probably occurs very near the energy of the $1t_{2g}$ orbital. Assigning the maxima of the two $L\alpha$ peaks to the $1t_{1g}$ and $1t_{2g}$ orbitals, we obtain a calculated separation of 3.8 ev, in good agreement with the experimental value of 4.2 ev. The peaks C and D at lower energy can be adequately correlated with the $1e_g$ and $5a_{1g}$ O 2*s* orbitals.

The O$K\alpha$ spectrum of TiO_2 shows a main peak which is accompanied by a shoulder at about 2.6 ev lower energy (Fischer, 1972; Smith and O'Nions 1972a). Since the seven highest filled orbitals all possess substantial O 2*p* character they should all contribute to the O$K\alpha$ spectrum. The position of the

O$K\alpha$ intensity maximum should correspond to some weighted average of the $1t_{1g}$, $6t_{1u}$, $1t_{2u}$, and $2e_g$ orbital positions. Simply weighting the energies of these four orbitals by their degeneracies, we calculate the O$K\alpha$ maximum to lie 1.1 ev lower in energy than the higher energy Ti$L\alpha$ peak. As shown in Fischer (1972), the experimental separation is 1.5 ev, in good agreement with the calculation. If the energies of the orbitals in the nonbonding and bonding sets are weighted by their degeneracies, an approximate separation of 3.4 ev between the peaks resulting from the two orbital sets and approximate main peak/shoulder intensity ratio of 11/7 is obtained, in fair agreement with experiment. An analogous weighting of the experimental energies from the UV photoelectron spectrum leads to a 3.2 ev separation. A more detailed analysis will require the calculation of spectral transition intensities.

The TiK, TiL, and OK X-ray absorption spectra all show similar features for TiO_2. This suggests that selection rules are greatly relaxed for transitions to conduction-band orbitals. The two low energy peaks (b and c) were assigned by Fischer to the $2t_{2g}$ and $3e_g$ orbitals. The experimental separation is 2.1 ev, somewhat smaller than the ~2.8 ev expected. However Fischer (1970) also finds a low value for $2t_{2g} - 3e_g$ splitting in Ti_2O_3 (1.9 ev *vs* 2.5 ev from optical spectra) and so the assignment seems sound. It is not clear why the X-ray $2t_{2g} - 3e_g$ splittings are systematically smaller than their optical values in these materials. Our calculated $2t_{2g} - 3e_g$ separation is somewhat larger (~3.6 ev). The peak d observed in the TiK absorption spectrum of Albrecht (1966) is assigned to the $7t_{1u}$ conduction-band orbital with the observed and calculated energies in good agreement. Unfortunately, the energy of the peak e falls outside the range of our calculations. On the whole, the various series of X-ray spectra are reproduced fairly well by the calculations.

Although our assignment of the TiL emission spectrum differs from that of Fischer, we agree that the $2t_{2g}\uparrow$ orbital, one third filled in Ti^{3+} oxides, will contribute intensity to the higher energy L emission peak. Therefore an increase in the relative intensity of the higher energy L emission peak does indicate an increasing amount of Ti^{3+}. Such an analysis was used by Pavicevic, Ramdohr, and ElGoresy (1972) to show the presence of Ti^{3+} in lunar ilmenites. They used the TiO_2 and Ti_2O_3 $L\alpha$ spectra of Fischer (1971) as reference spectra for Ti^{4+} and Ti^{3+} in octahedral coordination, noting that their pure ilmenite $L\alpha$ spectrum was very similar to Fischer's rutile spectrum.

The Electronic Structure and Spectra of Wustite, FeO, and Hematite, Fe_2O_3

MO Diagrams For FeO_6^{10-} *and* FeO_6^{9-}

The O 2s and valence MO structure of FeO_6^{10-}, the $X\alpha$ model for FeO, is shown in Figure 2a. The previously published (Tossell *et al*, 1973b) MO diagram for FeO_6^{9-} (the Fe_2O_3 model) is also shown (Fig. 2b) so as to permit comparisons between the Fe^{2+} and Fe^{3+} species. Since the iron oxides have ground states with total spins, $S \neq 0$, an unrestricted SCF calculation, in which the spin-up and spin-down electrons occupy different orbitals, must be per-

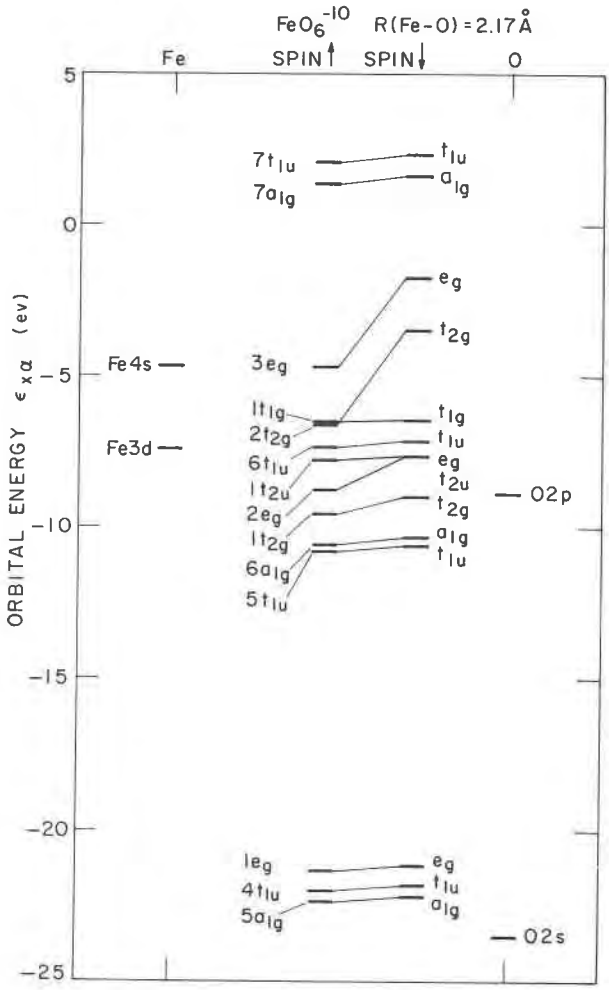

FIG. 2a. FeO_6^{10-} *MO* diagram (R(Fe — O) = 2.17 Å). The highest occupied orbital is the $2t_{2g}\downarrow$, containing one electron.

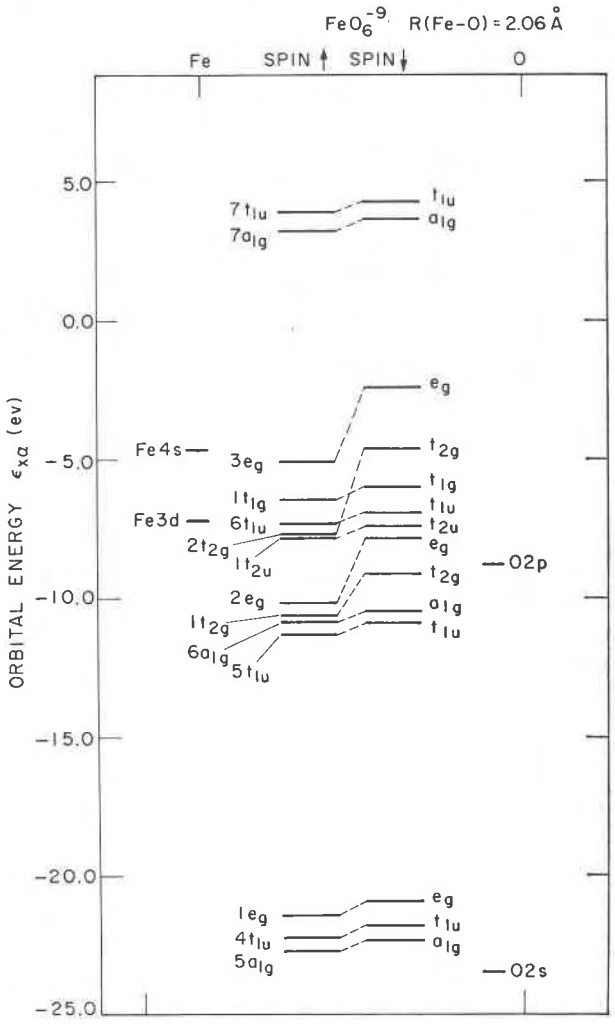

FIG. 2b. FeO_6^{9-} *MO* diagram (R(Fe — O) = 2.06 Å). The highest occupied orbital is the $3e_g\uparrow$, containing two electrons.

formed. Note that the spin splittings are quite large for the e_g and t_{2g} orbitals. The lowest-energy orbitals in Figure 2 are again the set of three predominantly O 2*s* orbitals. The $6a_{1g}$ and $5t_{1u}$ bonding orbitals have eigenvalues around −11 ev. We find the $1t_{2g}\uparrow$ and $2e_g\uparrow$ bonding orbitals around −9 ev in FeO_6^{10-} at higher energy than in FeO_6^{9-} by about 1 ev. The $1t_{1g}$, $6t_{1u}$, and $1t_{2u}$ orbitals are at about the same energy in both species and are again O 2*p* nonbonding orbitals. In the Fe^{2+} species the "crystal field" orbitals, $2t_{2g}$ and $3e_g$, are at or above the top of the O 2*p* nonbonding set while in the Fe^{3+} case the $2t_{2g}\uparrow$ orbital lies deeply within this set. The $2t_{2g}\uparrow \rightarrow 3e_g\uparrow$ eigenvalue difference is somewhat smaller in the ferrous case (1.7 *vs* 2.2 ev) and the spin-splitting is somewhat larger (2.9 *vs* 2.7 ev for the $3e_g$ state). The conduction band levels are lower than in TiO_2, and the FeO_6^{10-} conduction band levels are about 1.8 ev lower than those in FeO_6^{9-}. The difference in the energies of the crystal field levels with respect to the O 2*p* nonbonding orbitals is primarily a result of the difference in Fe oxidation state. The difference in conduction band levels results mainly from the oxidation state difference although the Fe-O distance (2.06 Å in FeO_6^{9-} and 2.17 Å in FeO_6^{10-}) also has some effect.

Valence region X-ray and UV photoelectron spectra are not available for FeO because of its instability with respect to Fe_2O_3. Therefore, the optical and X-ray emission spectra of ferrous compounds will be discussed first.

Optical Spectra for Octahedral Fe^{2+}

In oxide and silicate minerals in which ferrous iron is octahedrally coordinated, a crystal field $^5T_{2g} \rightarrow {}^5E_g$ transition with an average energy (Δ) of ~ 10,000 cm^{-1} (Burns, 1970) is normally observed. The "Δ_{VI}" value for R(Fe-O) = 2.17 Å is 9300 cm^{-1} from the analysis of Faye (1972). The value for the $2t_{2g}\downarrow \rightarrow 3e_g\downarrow$ transition from a transition state calculation is 13,700 cm^{-1}. This suggests an error in our calculated $2t_{2g}\downarrow \rightarrow 3e_g\downarrow$ separation of about 0.5 ev. Although this error is small in absolute magnitude, it is nonetheless a large percentage of the experimental result.[2] The lowest optically allowed $O^{2-} \rightarrow Fe^{2+}$ charge transfer transition is from $6t_{1u}\downarrow \rightarrow 2t_{2g}\downarrow$. The calculated transition-state energy is 37,500 cm^{-1} which compares well with experimental spectra which show an absorption edge around 35,000 cm^{-1} (Figgis, 1966). The lowest optical $L \rightarrow M$ charge transfer transitions in the ferric case are calculated to occur at 25,300 cm^{-1} ($6t_{1u} \rightarrow 2t_{2g}\downarrow$) and 29,400 cm^{-1} ($1t_{2u}\downarrow \rightarrow 2t_{2g}\downarrow$) and the transition is observed at 28,570 cm^{-1} (Tandon and Gupta, 1970). The lower value of the charge-transfer energy in Fe^{3+} oxides is a result of the lower relative energy of the crystal field orbitals in the ferric case. Very weak, spin-forbidden transitions are observed in Fe^{2+} minerals in the region from about 20–23,000 cm^{-1} (Burns, 1970, Fig. 3.2). The calculated transition-state energies of the $3e_g\uparrow$

[2] The observed SCF $X\alpha$ overestimation of the crystal field splitting by 0.5–0.8 ev in transition metal oxides can be eliminated by a slight modification of the procedures described in the "Calculational Method" section. Such modified calculations will be reported in the future.

$\rightarrow 3e_g\downarrow$ and $2t_{2g}\uparrow \rightarrow 2t_{2g}\downarrow$ transitions, 21,500 cm^{-1} and 22,400 cm^{-1} respectively, are in excellent agreement with experiment.

X-Ray Emission Spectra from Octahedral Iron

In Table 5, the calculated and experimental Fe $K\beta$ X-ray emission spectral energies of FeO and Fe_2O_3 are listed. In the Fe$K\beta$ spectra, the $K\beta'$ peak decreases in energy with respect to $K\beta_1$ as the oxidation state of iron increases, primarily because the $7t_{1u}$ orbital lies higher in the ferric state. This increase in the $K\beta'$-$K\beta_1$ separation from FeO to Fe_2O_3 was noted by Köster and Rieck (1970) and related to the larger d.c. resistivity of Fe_2O_3. The calculations also show that the $K\beta_5$ peak energy increases with an increase in the Fe oxidation state. This results from a drop in energy of the Fe 1s orbital while the 4, 5, and $6t_{1u}$ orbitals remain fairly constant in energy. This calculated trend is in agreement with experiment. The $K\beta_5'$ peak, arising from the $6t_{1u}$ O 2p nonbonding orbital is probably too weak to be observed in both FeO and Fe_2O_3.

It is observed experimentally that the Fe$K\beta$ absorption edge is ~5.8 ev higher in Fe_2O_3 than in FeO (Dodd and Glenn, 1968). We calculate the K absorption edge to lie higher in FeO_6^{9-} than in FeO_6^{10-} by 4.0 ev. This difference in energy arises from two separable but complementary effects: (1) the Fe 1s orbital is 2.2 ev lower with respect to the $1t_{1g}$ orbital in the Fe^{3+} case, (2) the $7t_{1u}$ conduction band orbital is 1.8 ev higher with respect to the $1t_{1g}$ in the Fe^{3+} case.

The Fe$L\alpha$ spectra of ferrous and ferric compounds are quite similar. A detailed assignment of the Fe_2O_3 $L\alpha$ emission and absorption spectra may be found in Tossell *et al* (1973b). Briefly, the main $L\alpha$ emission peak is assigned to the $2t_{2g}\uparrow$ orbital and the main absorption peak to $2t_{2g}\downarrow$. This assignment is consistent with the $2t_{2g}\uparrow \rightarrow 2t_{2g}\downarrow$ separation observed in the optical spectrum of Fe_2O_3. A weak peak on the high energy side of the $L\alpha$ emission peak, observable only under conditions of negligible self-absorption, has been assigned to the $3e_g\uparrow$ orbital. The low intensity of this peak is probably a result of self-absorption by the nearby $2t_{2g}\uparrow$ orbital. Alternatively, this high energy structure may be attributed to double ionization satellite intensity (Liefeld, 1968). The shoulder observed on the low energy side of the main $L\alpha$ emission peak is here assigned to orbitals $1t_{2g}\uparrow$ and/or $6a_{1g}$. If the primary intensity of this shoulder arises from $1t_{2g}\uparrow$, then its energy with respect to the main peak will have little dependence on Fe oxidation state. On the other hand, if the $6a_{1g}$ yields appreciable intensity, the separation of the shoulder from the main peak should increase from ferrous to ferric compounds. At present, no experimental information exists on this point. By analogy with TiO_2, low energy satellite peaks arising from the predominantly O 2s MO's, namely $1e_g$ and $5a_{1g}$, are expected. Calculated energies of these orbitals indicate an ~1 ev smaller separation of the O 2s derived peaks and the main peak in ferric state relative to the ferrous. This is a consequence of the lower relative $2t_{2g}\uparrow$ energy for Fe^{3+}. Apparently, no attempt has been made to observe features in this region of the Fe$L\alpha$ spectrum.

TABLE 5. Experimental and Calculated Fe$K\beta$ X-ray Emission Spectra: FeO *vs* Fe_2O_3 (*energies in ev*)

	FeO		Fe_2O_3		
Peak label	Experimental relative E[a]	Calculated relative E	Experimental relative E[a]	Calculated relative E	MO assignment
$K\beta'$	-13.4	-11.3	-14.3	-13.4	$3t_{1u}\rightarrow$Fels - ($1t_{2g}\downarrow\rightarrow 7t_{1u}\downarrow$)
$K\beta_{1,3}$	0	0	0	0	$3t_{1u}\rightarrow$Fels
$K\beta$ "	33.0	32.8	34.2	34.6	$4t_{1u}\rightarrow$Fels
$K\beta_5$	47.4	44.0	48.1	45.5	$5t_{1u}\rightarrow$Fels
$K\beta_5'$		47.4		49.5	$6t_{1u}\rightarrow$Fels
$K\beta''$		56.8	61.7	60.9	$7t_{1u}\rightarrow$Fels

[a] Koster and Mendel (1970).

The ratio of the $L\beta/L\alpha$ peak intensity decreases linearly and quantitatively as iron oxidation state increases within some solid solution series (O'Nions and Smith, 1971; Pavicevic *et al*, 1972). O'Nions and Smith (1971) explain this by assuming that the $L\beta$ peak arises from transitions from antibonding MO's only (*e.g.*, $2t_{2g}\uparrow$) while both antibonding ($2t_{2g}\uparrow$) and bonding (*e.g.*, $2e_g$, $1t_{2g}$, $6a_{1g}$, $5t_{1u}$) MO's contribute to $L\alpha$. However, it is apparent from the shape of the $L\alpha$ spectra (O'Nions and Smith, 1971) that even if this assumption were true, the percent of the $L\alpha$ intensity arising from the bonding orbitals is quite small (certainly <10 percent). An alternative explanation is that in Fe^{3+} compounds, there is a preferential self-absorption of the $L\beta$ peak. This interpretation is supported by our calculations (Fig. 3). Features in the $L\alpha$ absorption spectrum result from transitions from the Fe $2p_{3/2}$ state to the crystal-field-type orbitals $2t_{2g}\downarrow$ and $3e_g\downarrow$ and the conduction band orbital $7a_{1g}$ (and perhaps $7t_{1u}$). These spectral features are shown strikingly in Fischer's Cr oxide X-ray absorption spectra (Fischer, 1971). The separation of the $L\alpha$ and $L\beta$ absorption maxima in Fe oxides is ~11.2 ev at 2 kV operating voltage (O'Nions and Smith, 1971). The $2t_{2g}\downarrow$ and $3e_g\downarrow$ orbitals are at the right energy to absorb X-ray intensity on the high energy side of the $L\alpha$ emission peak in both the Fe^{2+} and Fe^{3+} cases. On the other hand, the $7a_{1g}$ and $7t_{1u}$ conduction band orbitals for Fe^{2+} occur at a minimum in the emission spectra (between the $L\alpha$ and $L\beta$ peaks) while in Fe^{3+} compounds the conduction band orbitals fall right on top of the $L\beta$ emission peak. Therefore the $L\beta$ peak will be preferentially self-absorbed in Fe^{3+} compounds to produce lower $L\beta/L\alpha$ intensity ratios.

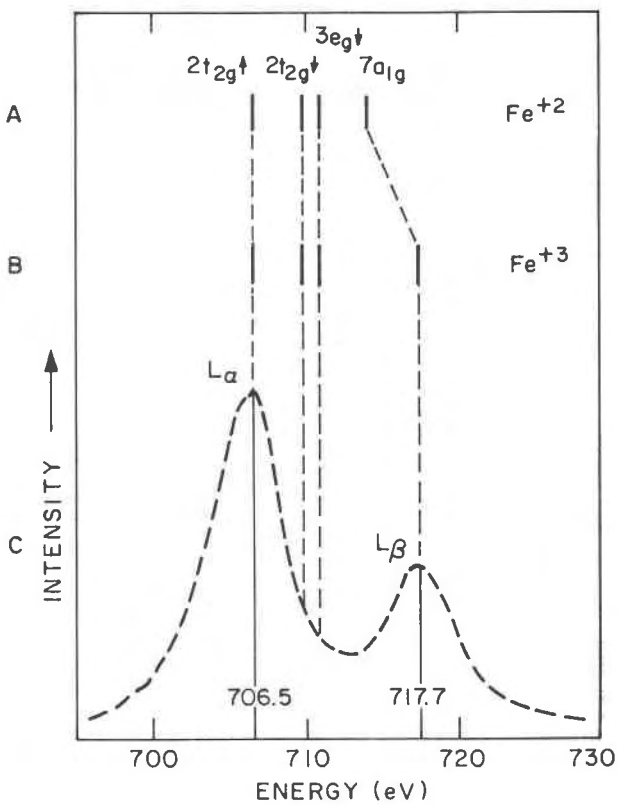

FIG. 3. Experimental Fe $L\alpha,\beta$ X-ray emission spectrum of Fe_2O_3 and calculated $X\alpha$ energies of empty MO's generating $L\alpha$ absorption peaks in Fe^{2+} and Fe^{3+} oxides.
A. FeO_6^{10-} empty orbital energies
B. FeO_6^{9-} empty orbital energies
C. Fe_2O_3 $L\alpha,\beta$ spectrum (O'Nions and Smith, 1971)

The separation of the $2t_{2g}\uparrow$ and $7a_{1g}\uparrow$ orbitals is mainly a function of oxidation state although preliminary SCF $X\alpha$ results do show it to have a weak metal-oxygen distance dependence. Therefore the $L\beta/L\alpha$ intensity ratio does measure the percent Fe^{3+}. Fischer and Baun (1968) have explained how such a technique ("differential self-absorption") can be used to obtain L absorption spectra explicitly, and Dodd and Ribbe (1972) have obtained preliminary results for minerals.

In the $OK\alpha$ spectra of the iron oxides, experiment shows a broad peak at 524.6 ev in hematite and, in wustite, a main peak at 524.1 ev with a shoulder at 527.2 ev (Smith and O'Nions, 1972a). Our calculation on the ferric cluster shows the crystal field and O $2p$ nonbonding and bonding orbitals to be fairly well mixed in energy, thus explaining the broad featureless spectrum observed in Fe_2O_3. On the other hand, in the ferrous case the $3e_g\uparrow$ and $2t_{2g}$ orbitals are well separated from the O $2p$ nonbonding levels, as shown in Figure 2a. The 2.8 ev separation between the weighted average energies of the O $2p$ nonbonding orbitals (plus the $2t_{2g}\uparrow$ and $2e_g\downarrow$) and the $3e_g\uparrow$, $2t_{2g}\downarrow$ crystal field orbitals compares well with the experimental separation of 3.1 ev. Therefore the $OK\alpha$ X-ray emission spectrum of wustite shows a high energy shoulder directly attributable to the Fe^{2+} crystal field orbitals.

Although no valence region photoelectron spectra are available for FeO, the valence region photoelectron spectrum of Fe_2O_3 has been interpreted with fair success (Tossell *et al*, 1973b). The separation of the upper valence orbitals and the O $2s$ orbitals was calculated within an accuracy of about 1 ev and the upper valence region was reproduced reason-

ably well. The crystal field splitting of the $2t_{2g}\uparrow$ and $3e_g\uparrow$ orbitals was a prominent feature of the experimental spectrum. The measured crystal field splitting was ~1.9 ev or about 15,000 cm^{-1}, in reasonable agreement with the measured values of 13,700–16,500 cm^{-1} for 10 Dq in octahedral ferric compounds (Burns, 1970, Table 2.4). The separation we calculated was somewhat larger, about 2.7 ev. The only ambiguous feature in the spectrum, a peak around 15 ev in binding energy, is now believed due to photoemission by the Mg$K\alpha_{3,4}$ satellite line from the Mg$K\alpha$ X-ray. Calabrese and Hayes (1973) have shown for a series of transition metal oxides that the spectral region shows only weak satellite intensity. The study of the valence region X-ray (or UV) photoelectron spectrum of a stable ferrous mineral such as fayalite would provide a good test for our FeO_6^{10-} calculation. The fayalite photoelectron spectrum should be interpretable in terms of a superposition of the calculated spectra of the FeO_6^{10-} and SiO_4^{4-} polyhedra.

Transition Metal Oxides: Elucidation of Structures from Spectral Data

In the iron and titanium oxides, the non-core orbitals can be divided into: (1) a set of O 2s nonbonding orbitals ($5a_{1g}$, $4t_{1u}$, $1e_g$); (2) a set of metal-oxygen bonding orbitals with substantial density in the interatomic region ($5t_{1u}$, $6a_{1g}$, $1t_{2g}$, $2e_g$); (3) a set of O 2p nonbonding orbitals ($1t_{2u}$, $6t_{1u}$, $1t_{1g}$); (4) the "crystal field" orbitals ($2t_{2g}$, $3e_g$) with metal 3d and O 2p character; and (5) the conduction band orbitals ($7a_{1g}$, $7t_{1u}$) which are metal-oxygen 4s and 4p antibonding and diffuse in character. The orbital sets most affecting the stability of the system are the bonding and the crystal field sets. The O 2s and O 2p nonbonding sets are quite constant in energy while the conduction band set is empty and therefore does not affect the ground state energy.

The energies of the various orbital sets may be determined experimentally in the following manner. The O 2s orbitals are most easily identified by X-ray photoelectron spectroscopy. In conjunction with a photoelectron measurement of the M 3s or 3p level they could give useful information on the charge distribution in the M-O bond. Measuring binding energies of M and O orbitals together would eliminate the problems of charging and reference level effects and greatly simplify comparison of calculated and observed photoelectron shifts. The O 2s orbitals can also be identified in $MK\beta$ X-ray emission spectra and perhaps in ML spectra. The energy of the O 2s derived $K\beta$ spectral peaks (and perhaps the L peaks) are good indicators of the transition metal's oxidation state.

The metal-oxygen bonding orbitals, although very interesting, are most difficult to locate experimentally. The best method for studying them appears to be $MK\beta$ X-ray emission spectroscopy, but the appropriate peak ($K\beta_5$) is very weak. These orbitals may be resolvable in O$K\alpha$ spectra if they are fairly compact and well separated from the O 2p nonbonding orbitals (as in TiO_2). Also, since the bonding orbitals are quite diffuse, they should show substantial intensity in UV photoelectron spectra for reasons discussed by Lohr and Robin (1970) (this is the case in TiO_2). In many cases, the structure of the bonding orbitals may also be seen in the UV reflectance spectrum.

The O 2p nonbonding levels are easily found from O$K\alpha$ X-ray emission spectroscopy. Although they show little variation in energy for the clusters studied here, this may be due to the length of the O–O edges. The shortest O–O edge in any of the clusters studied was 2.76 Å. At smaller distances, it is conceivable that O–O antibonding does cause a substantial rise in the energy of this orbital set. Note that it is precisely this effect which is the basis of the radius ratio rules.

As is well known, the "crystal field" orbitals are most easily studied by optical absorption and reflectance spectroscopy. Transitions within the crystal field set as well as transitions from the O 2p nonbonding set (and in some cases the M-O bonding set) to the crystal field orbitals can be thus studied. The crystal field orbitals can also be studied by X-ray photoelectron spectroscopy and X-ray absorption spectroscopy. The conduction band levels can best be studied by far UV spectroscopy but can also be studied usefully by $MK\beta$ X-ray emission spectroscopy. Therefore, every set of levels can be studied spectroscopically.

Spectral Evaluation of Mineral Stability

A worthwhile goal would be to evaluate the stability of a transition metal-oxygen cluster directly from the spectroscopic values of the energy levels. One major problem in implementing this procedure at the present time is the difficulty in studying the M–O bonding orbital set, since these orbitals are spread out in energy and diffuse in space (thus generating fairly small X-ray intensities). A second

serious problem is in the very high spectral energy resolution required. An average error of only 0.1 ev in FeO_6^{10-} valence orbital energy would produce an error in total energy of ~16 kcal/Fe–O bond.

Of course, in most cases, it is not the total energy of a system but rather the relative energies of related systems which are of interest. For related systems, it is possible that the energy variations in one of the orbital sets will essentially determine the relative energies or stabilities. This will certainly be the case if all the other orbital sets are constant in energy. It will also occur if the energy variations of the other orbital sets compensate for each other. For example, qualitative considerations and preliminary SCF $X\alpha$ calculations show clearly that reducing the Fe–O distance will destabilize the crystal field orbitals (*i.e.*, raise their energy baricenter), stabilize the bonding orbitals, and increase the crystal field splitting). The total energy will be a complicated function of all these effects. Oxygen-oxygen antibonding effects may also be important in some cases. As noted by Burns (1970), crystal field stabilization energies are a small fraction of total lattice energies (usually <10 percent) but have a strong influence upon relative stabilities and thus are good predictors of element fractionation and site enrichment. This is understandable in terms of the competition between crystal field orbital destabilization and bonding orbital stabilization. It is possible that a model which included the crystal field splitting, the separation of the O $2p$ nonbonding and crystal field levels, and the energy of one of the bonding orbitals would give accurate relative stabilities in all cases, and thus be able to predict element fractionations and site enrichments. Such a model would require experimental data from optical absorption spectra for crystal field splittings, from UV reflectance spectra for accurate $O^{2-} \rightarrow$ Fe charge transfer energies, and from Fe$K\beta$ and L (or in simple minerals O$K\alpha$) X-ray emission spectra for bonding orbital energies.

Prediction of the Spectra and Electronic Structure of Minerals at High Pressures

An important area of application of these results is in the interpretation and prediction of the spectra and electronic state of Fe in minerals at high pressure. Methods have been developed by Gaffney (1972) and by Wood and Strens (1972) for calculating crystal field spectra from crystal structure data. These methods, which rely upon an assumed R^{-5} distance-dependence law for the crystal field splitting and upon empirical parameterization, yield crystal field spectra in fairly good agreement with experiment. However, the high pressure optical and conductivity studies of Mao and Bell (1972) indicate that the major change in the high pressure spectrum of fayalite (in both olivine and spinel polymorphs) is an enormous reduction in energy and an increase in intensity of the O $\rightarrow$ Fe charge transfer band. Such changes are outside the scope of semi-empirical crystal field calculations. Similar shifts in the $O^{2-} \rightarrow Fe^{3+}$ charge transfer peak of Fe^{3+} chemical compounds have been observed by Drickamer and correlated with $Fe^{3+} \rightarrow Fe^{2+}$ reduction observed at high pressure by Mössbauer spectroscopy (Drickamer and Frank, 1972). A similar reduction of Fe^{3+} to Fe^{2+} has been observed in the mineral magnesioriebeckite (Burns, Tossell, and Vaughan, 1972). SCF $X\alpha$ calculations are presently being performed on Fe–O clusters at different Fe–O distances in order to interpret those results.

Acknowledgments

We thank R. G. Burns for a critical reading of this manuscript, and T. L. Gilbert and G. K. Wertheim for copies of their manuscripts in advance of publication. This research was supported by the National Aeronautics and Space Administration under Grant no. NGL 22-009-187, and by the National Science Foundation through the M.I.T. Center for Materials Sciences and Engineering.

References

ADAMS, I., J. M. THOMAS, AND G. M. BANCROFT (1972) An ESCA study of silicate minerals. *Earth Planet. Sci. Lett.* **16,** 429–432.

ALBEE, A. L., AND A. A. CHODOS (1970) Semiquantitative electron microprobe determination of Fe^{2+}/Fe^{3+} and Mn^{2+}/Mn^{3+} in oxides and silicates and its application to petrologic problems. *Am. Mineral.* **55,** 491–501.

ALBRECHT, G. (1966) *Röntgenspectrken und Chemische Bindung,* p. 3, Karl Marx Univ., Leipzig (reproduced in Fischer, 1972).

BETHE, H. (1929) Splitting of terms in crystals. *Ann. Phys.* **3,** 133–206.

BLOKHIN, M. A., AND A. T. SHUVAEV (1962) Concerning the influence of the chemical bonds on the X-ray emission spectrum of titanium. *Bull. Acad. Sci. (USSR) Phys. Ser.* **26,** 429–432 (reproduced in Fischer, 1972).

BURNS, R. G. (1970) *Mineralogical Applications of Crystal Field Theory*. Cambridge Univ. Press, Cambridge, England.

———, AND W. S. FYFE (1967) Crystal field theory and the geochemistry of transition elements. In P. H. Abelson, Ed., *Researches in Geochemistry,* **2,** J. Wiley and Son, New York, pp. 259–285.

———, J. A. TOSSELL, AND D. J. VAUGHAN (1972) Pressure-induced reduction of a ferric amphibole. *Nature,* **240,** 33–35.

CALABRESE, A., AND R. G. HAYES (1973) Studies of the valence electron levels of CrO_4^{2-}, $Cr_2O_7^{2-}$, MnO_4^-, VO_4^{3-} and FeO_4^{2-} by X-ray photoelectron spectroscopy. *J. Am. Chem. Soc.* **95,** 2819–2822.

CARDONA, M., AND G. HARBEKE (1965) Optical properties and band structure of wurtzite-type crystals and rutile. *Phys. Rev.* **137,** A1467–1476.

CARVER, J. C., G. K. SCHEWEITZER, AND T. A. CARLSON (1972) Use of X-ray photoelectron spectroscopy to study bonding in Cr, Mn, Fe, and Co compounds. *J. Chem. Phys.* **57,** 973–982.

CLACK, D. W., N. S. HUSH, AND J. R. YANDLE (1972) All-valence electron CNDO calculations on transition-metal complexes. *J. Chem. Phys.* **57,** 3503–3510.

COLLINS, G. A. D., D. W. J. CRUICKSHANK, AND A. BREEZE (1972) *Ab initio* calculations on the silicate ion, orthosilicic acid and their $L_{2,3}$ X-ray spectra. *J. Chem. Soc. Faraday Trans.* **68,** 1189–1195.

COTTON, F. A., AND G. WILKINSON (1972) *Advanced Inorganic Chemistry,* 3rd. ed. Interscience Publ., New York.

CRONEMEYER, D. C. (1952) Electrical and optical properties of rutile single crystals. *Phys. Rev.* **87,** 876–886.

DERBENWICK, G. F. (1970) *Stanford Electronic Laboratories Technical Rep.* **#5220-2.**

DISTEFANO, T. H., AND D. E. EASTMAN (1971) Photoemission measurements of the valence levels of amorphous SiO_2. *Phys. Rev. Lett.* **27,** 1560–1562.

DODD, C. G., AND G. L. GLENN (1968) Use of MO theory to interpret X-ray *K*-absorption spectral data. *J. Appl. Phys.* **39,** 5372–5377.

———, AND ——— (1969) A study of chemical bonding in silicate minerals by X-ray emission spectroscopy. *Am. Mineral.* **54,** 1299–1311.

———, AND P. H. RIBBE (1972) Improved electron microprobe measurement of Fe^{+2}/Fe^{+3} using Fe L_{II-III} band spectra (abstr.). *Geol. Soc. Am. Abstr. Programs,* **4,** 488–489.

DRICKAMER, H. G., AND C. W. FRANK (1972) Electronic structure, electron transitions and the high pressure chemistry and physics of solids. *Ann. Rev. Phys. Chem.* **23,** 39–64.

FAYE, G. H. (1972) Relationship between crystal field splitting parameter, "Δ_{VI}", and M_{host}—O bond distance as an aid in the interpretation of absorption spectra of Fe^{2+}—bearing minerals. *Can. Mineral.* **11,** 473–487.

FIGGIS, B. N. (1966) *Introduction to Ligand Fields.* Interscience Publ., New York.

FISCHER, D. W. (1970) MO interpretation of the soft X-ray $L_{II,III}$ emission and absorption spectra of some titanium and vanadium compounds. *J. Appl. Phys.* **41,** 3561–3569.

——— (1971) Soft X-ray band spectra and molecular orbital structure of Cr_2O_3, CrO_3, CrO_4^{-2} and $Cr_2O_7^{-2}$. *J. Phys. Chem. Solids,* **32,** 2455–2480.

——— (1972) X-ray band spectra and MO structure of rutile, TiO_2. *Phys. Rev. B, Solid State,* **5,** 4219–4226.

———, AND W. L. BAUN (1968) Band structure and the Ti $L_{II,III}$ X-ray emission and absorption spectra from pure metal, oxides, nitride, carbide, and boride. *J. Appl. Phys.* **39,** 4757.

GAFFNEY, E. S. (1972) Crystal field effects in mantle minerals. *Phys. Earth Planet. Interiors,* **6,** 385–390.

———, AND T. J. AHRENS (1970) Stability of mantle minerals from lattice calculations and shock wave data. *Phys. Earth Planet. Interiors,* **3,** 205–212.

GILBERT, T. L., W. J. STEVENS, H. SCHRENK, M. YOSHIMINO, AND P. S. BAGUS (1973) Chemical bonding effects in the oxygen $K\alpha$ X-ray emission bands of silica. *J. Chem. Phys.* (in press).

GRANT, F. A. (1959) Properties of rutile (titanium dioxide). *Rev. Mod. Phys.* **31,** 646–674.

HÜFNER, S., AND G. K. WERTHEIM (1973) X-ray photoelectron band structure of some transition metal compounds. *Phys. Rev.* **B 9,** 4857–4867.

HUNTRESS, W. T. JR., AND L. WILSON (1972) An ESCA study of lunar and terrestrial materials. *Earth Planet Sci. Lett.* **15,** 59–69.

HUZINAGA, S., AND C. ARNAU (1971) Virtual orbitals in Hartree-Fock theory. II. *J. Chem. Phys.* **54,** 1948–1951.

JOHNSON, K. H. (1973) Scattered wave theory of the chemical bond. *Adv. Quant. Chem.* **7,** 143–185.

———, AND F. C. SMITH, JR. (1972) Chemical bonding of a molecular transition metal ion in a crystalline environment. *Phys. Rev.* **B 5,** 831–843.

KAHN, A. H., AND A. J. LEYENDECKER (1964) Electronic energy bands in $SrTiO_3$. *Phys. Rev.* **135,** A1321–1325.

KLEIN, G., AND H. U. CHUN (1972) Determination of optical interband transitions in crystalline quartz from X-ray spectroscopic data. *Phys. Status Solidi,* **(B) 49,** 167–172.

KÖSTER, A. S., AND H. MENDEL (1970) X-ray $K\beta$ emission spectra and energy levels of compounds of 3*d* transition metals—I. Oxides. *J. Phys. Chem. Solids,* **31,** 2511–2522.

———, AND G. D. RIECK (1970) Determination of valence and coordination of iron in oxidic compounds by means of the iron X-ray fluorescence emission spectrum. *J. Phys. Chem. Solids,* **31,** 2505–2510.

LANDOLT-BÖRNSTEIN (1955) *Zahlenwerte und Funktionen,* Vol. 1, p. 4, Springer, Berlin.

LIEFELD, R. G. (1968) Soft X-ray emission spectra at threshold excitation. In *Soft X-ray Band Spectra,* Ed. D. J. Fabian. Academic Press.

LOHR, L. L. JR., AND M. B. ROBIN (1970) Theoretical study of photoionization cross sections for π-electron systems. *J. Am. Chem. Soc.* **92,** 7241–7247.

LOUISNATHAN, S. J., AND G. V. GIBBS (1972) The effect of tetrahedral angles on Si-O bond overlap populations for isolated tetrahedra. *Am. Mineral.* **57,** 1614–1642 (and companion papers).

MANNING, P. G. (1970) Racah parameters and their relationship to lengths and covalencies of Mn^{2+} and Fe^{3+}-oxygen bonds in silicates. *Can. Mineral.* **10,** 677.

MAO, H. K., AND P. M. BELL (1972) Electrical conductivity and the red shift of absorption in olivine and spinel at high pressure. *Science,* **176,** 403–406.

MOSKOWITZ, J. W., C. HOLLISTER, C. J. HORBECK, AND H. BASCH (1970) SCF study of the cluster model in ionic salts. I. NiF_6^{4-}. *J. Chem. Phys.* **53,** 2570–2580.

NORDLING, C. (1972) ESCA: Electron spectroscopy for chemical analysis. *Angew.* (Int. ed.) **II,** 83–92.

O'NIONS, R. K., AND D. G. SMITH (1971) Investigations of the $L_{II,III}$ X-ray emission spectra of Fe by electron

microprobe, part 2. The Fe $L_{II,III}$ spectra of Fe and Fe-Ti oxides. *Am. Mineral.* **56,** 1452–1463.

ORGEL, L. E. (1952) The effects of crystal fields on the properties of transition metal ions. *J. Chem. Soc.* 4756–4761.

——— (1960) *An Introduction to Transition Metal Chemistry Ligand Field Theory.* John Wiley and Sons, Inc., New York.

PAULING, L. (1929) The principles determining the structure of complex ionic crystals. *J. Am. Chem. Soc.* **51,** 1010–1026.

——— (1960) *The Nature of the Chemical Bond,* 3rd. ed. Cornell University Press, Ithaca, New York.

PAVICEVIC, M., P. RAMDOHR, AND A. ELGORESY (1972) Electron microprobe investigations of the oxidation states of Fe and Ti in ilmenite in Apollo 11, 12, and 14 crystalline rocks. *Geochim. Cosmochim. Acta, Supplement 3,* **1,** 295–303.

PRINS, R., AND T. NOVAKOV (1972) Valence region X-ray photoelectron spectra of MnO_4^- and CrO_4^{2-}. *Chem. Phys. Lett.* **16,** 86–88.

ROOTHAAN, C. C. J. (1951) New developments in MO theory. *Rev. Mod. Phys.* **23,** 69–89.

SHIRLEY, D. A., Ed. (1970) *Electron Spectroscopy.* North-Holland Publ. Co., Amsterdam.

SLATER, J. C. (1972) Statistical exchange-correlation in the self-consistent field. *Adv. Quant. Chem.* **6,** 1–92.

———, AND K. H. JOHNSON (1972) Self-consistent field $X\alpha$ cluster method for polyatomic molecules and solids. *Phys. Rev.* **B 5,** 844–853.

SMITH, D. G. W., AND R. K. O'NIONS (1972a) Investigations of bonding in some oxide minerals by oxygen $K\alpha$ emission spectroscopy. *Chem. Geol.* **9,** 29–43.

———, AND ——— (1972b) Investigations of bonding by $OK\alpha$ emission spectroscopy: further evidence concerning the true character of the oxygen $K\alpha$ emission band. *Chem. Geol.* **9,** 145–146.

TANDON, S. P., AND J. P. GUPTA (1970) Diffuse reflectance spectrum of ferric oxide. *Spectrosc. Lett.* **3,** 297–301.

TOSSELL, J. A. (1973a) Molecular orbital interpretation of X-ray emission and ESCA spectral shifts in silicates. *J. Phys. Chem. Solids,* **34,** 307–319.

——— (1973b) Interpretation of K X-ray emission spectra and chemical bonding in oxides of Mg, Al, and Si using quantitative molecular orbital theory. *Geochim. Cosmochim. Acta,* **37,** 583–594.

———, D. J. VAUGHAN, AND K. H. JOHNSON (1973a) X-ray photoelectron X-ray emission and UV spectra of SiO_2 calculated by the SCF $X\alpha$ scattered wave method. *Chem. Phys. Lett.* **20,** 329–334.

———, ———, AND ——— (1973b) The electronic structure of ferric iron octahedrally coordinated to oxygen: a fundamental polyhedral unit of iron bearing oxide and silicate minerals. *Nature,* **244,** 42–45.

URCH, D. S. (1970) The origin and intensities of low energy satellite lines in X-ray emission spectra: a molecular orbital interpretation. *J. Phys. C. Solid State Phys.* **3,** 1275–1291.

——— (1971) X-ray emission spectroscopy. *Quart. Rev.* **25,** 343–364.

VAUGHAN, D. J., AND J. A. TOSSELL (1973) Molecular orbital calculations on Be and B oxyanions: Interpretation of X-ray emission, ESCA and NQR spectra and of the geochemistry of Be and B. *Am. Mineral.* **58,** 765–770.

———, ———, AND K. H. JOHNSON (1974) The bonding of ferrous iron to sulfur and oxygen in tetrahedral coordination: A comparative study using SCF $X\alpha$ scattered wave molecular orbital calculations. *Geochim. Cosmochim. Acta* (in press).

WERME, L. O., B. GRENNBERG, J. NORDGREN, C. NORDLING, AND K. SIEGBAHN (1973) Observation of vibrational fine structure in X-ray emission lines. *Phys. Rev. Lett.* **30,** 523–524.

WOOD, B. J., AND R. G. J. STRENS (1972) Calculation of crystal field splittings in distorted coordination polyhedra: spectra and thermodynamic properties of minerals. *Mineral. Mag.* **38,** 909–917.

Manuscript received, July 2, 1973; accepted for publication, September 27, 1973.